Water Air Soil Pollut (2013) 224:1757
DOI 10.1007/s11270-013-1757-0

Inhibition of Acid Mine Drainage from a Pyrite-rich Mining Waste Using Industrial By-products: Role of Neo-formed Phases

P. K. Sahoo · S. Tripathy · M. K. Panigrahi · Sk. Md. Equeenuddin

Received: 25 April 2013 / Accepted: 16 September 2013 / Published online: 8 October 2013

Abstract In the present study, the potential use of the industrial waste residues, such as coal fly ash and clinker dust, was evaluated in inhibiting acid mine drainage generation from pyrite-rich wastes using non-saturated column experiments. Two columns (B and C) were filled with a mixture of industrial residues over pyrite-quartz sand (PS), while one column (A) used as the control was solely filled with PS. Artificial irrigation was maintained in each column by pouring Milli-Q water (pH 6.5). The leachate chemistry and the precipitation of neo-formed phases in the columns were examined. Based on the pH and concentration of SO_4^{2-} in the effluent collected over a period of time, it can be inferred that pyrite dissolution was dominant in column A. In columns B and C, the addition of industrial waste produced a near neutral to alkaline leachate. At this pH, Fe released from pyrite oxidation was immediately depleted by precipitating into Fe-oxyhydroxide phases that likely coated the pyrite grains (termed as microencapsulation) which inhibited oxidation. This was supported from the scanning electron microscope observation and the geochemical modeling results. In addition, the precipitation of other neo-formed phases such as calcium carbonate and gypsum, along with the pozzolanic reactions of industrial wastes, possibly increased the cementation of fly ash particles leading to the development of a compact material, which prevented further oxidation by restricting infiltration and oxygen contact to the pyrite surface. This occurred best in column B; thus, it produced better quality of leachates than column C, though at the end both columns showed a significantly decreased concentration of Fe (up to 99.9 %) and other metals such as Cu, Cr, Pb, Zn, and Mn (lower values than the WHO permissible limits of drinking water) compared to control.

Keywords Acid mine drainage · Fly ash · Pyrite oxidation · Secondary precipitate · Microencapsulation

P. K. Sahoo (✉)
Vale Institute of Technology Sustainable Development, Boaventura da Silva, 66055-090 Belém, Pará, Brazil
e-mail: prafulla.sahoo@vale.com

P. K. Sahoo · S. Tripathy (✉) · M. K. Panigrahi
Department of Geology & Geophysics, Indian Institute of Technology, Kharagpur 721302 West Bengal, India
e-mail: stripathy@iitbbs.ac.in

S. Tripathy
School of Earth, Ocean and Climate Sciences, Indian Institute of Technology, Bhubaneswar 751013, India

S. M. Equeenuddin
Department of Mining Engineering, National Institute of Technology, Rourkela 769008 Odisha, India

1 Introduction

Acid mine drainage (AMD) is one of the biggest environmental problems facing the mining industry globally (Akabzaa et al. 2007). AMD occurs when sulfide minerals, mainly pyrite associated with mining wastes or overburden as a consequence of mining, gets oxidized in

the presence of atmospheric moisture (Lottermoser 2007; Sahoo et al. 2012a). The detailed mechanism of pyrite oxidation was suggested by Singer and Stumm (1970). In brief, pyrite is initially oxidized by atmospheric O_2, releasing Fe^{2+}, SO_4^{2-}, and H^+. The Fe^{2+} thus produced is further oxidized by O_2 into Fe^{3+}. Under acidic condition (pH <3), Fe^{2+} is rapidly oxidized by *Thiobacillus ferrooxidans* to Fe^{3+}, which oxidizes pyrite at a much faster rate than O_2 (Singer and Stumm 1970). The resulting acidic drainage from pyritic materials reacts with country rocks (containing ferromagnesian and aluminosilicate minerals) and may contribute significant amounts of Fe, Al, SO_4^{2-}, and toxic metals to the drainage that leads to the contamination of surface and groundwater bodies and threats living beings (Equeenuddin et al. 2010; Nordstrom and Alpers 1999; Ji et al. 2007; Pelo et al. 2009). Thus, the control of AMD production from such sources has been a major challenge in the recent years.

Several strategies have been focused to prevent the generation of AMD from sulfide-bearing materials (Kleinmann 1990; Evangelou 1995; Johnson and Hallberg 2005). The most common approaches are the creation of oxygen barrier using soil and water cover to minimize the penetration of oxygen into sulfide residues (Yanful et al. 2000; Vigneault et al. 2001; Vandiviere and Evangelou 1998) or the use of bactericides to inhibit bacterial action (Kleinmann 1998). However, these techniques are effective on short term and need high maintenance cost. In contrast, a recently proposed technology, i.e., microencapsulation, in which the coating of pyrite grains with a substance blocks transport of oxidants to the grain surface is relatively effective and a promising technique to reduce the rate of oxidation (Evangelou 2001). Several types of coatings have been proposed including inorganic coating such as ferric phosphate (Nyavor and Egiebor 1995) and ferric hydroxide-silica (Zhang and Evangelou 1998) and organic coating such as phospholipids (Kargbo et al. 2004), oxalic acid (Belzile et al. 1997), humic acids (Ačai et al. 2009), and polyethylene polyamine (Cai et al. 2005). These coatings have been found to be effective in inhibiting pyrite oxidation in the laboratory, but their field application is restricted due to high reagent cost and further deleterious impacts on the environment. For example, some organic reagents, such as polyamine, oxalic acid, and iron 8-hydroxyquinoline, are toxic to aquatic life, while inorganic reagent, such as PO_4, leads to eutrophication. In addition, these materials are not self-healing and permanent; thus, they require a long-term commitment to site management. In comparison, coating of pyrite with inorganic coating such as Fe-oxyhydroxides by means of locally available waste material such as fly ash would be more effective due to its low cost and self-healing capacity (Tasse et al. 1997; Pérez-López et al. 2007a). This material is also able to bind with inert solid particles and make a hardened material by forming some neo-formed phases (Pérez-López et al. 2007b, c). Furthermore, the use of site-specific and easily availability waste material in preventing AMD is twice beneficial from an environmental point of view.

Tertiary coal deposits in many parts of the world, rich in Fe sulfide minerals in the coal seams and intercalated sedimentary strata, pose a significant threat to the environment by generating AMD (Perry and Brady 1995; Campbell et al. 2001). Jaintia Hills coalfield in the northeastern state of Meghalaya, India is one of them. The Jaintia Hills coalfield is the major coal-producing zone in the state of Meghalaya, India, where the coal seams and associated strata contain significant amounts of pyrite that is responsible for the generation of AMD in the area (Sahoo et al. 2012a, 2013). The AMD from this coalfield is contaminating surrounding water bodies which may affect the human and livestock population (Sahoo 2011). Thus, there is an urgent need to control the AMD production in the Jaintia Hills.

The main aim of this study is to investigate the utilization of the mixture of fly ash and clinker dust to inhibit the oxidation of pyrite in coal mine wastes. The idea is to produce alkaline pH and subsequent precipitation of Fe-oxyhydroxides and to verify the effectiveness of Fe-oxyhydroxide coating on sulfide surface along with precipitation of other neo-formed phases in inhibiting oxidation process.

2 Materials and Methods

2.1 Collection of Materials

The sulfide-rich samples used in this study were collected from the coal dumping site of the Jaintia Hills coalfield, Meghalaya. The sample was air dried and ground to a particle size of 100–500 μm. Industrial waste residues, fly ash and clinker dust, were obtained from the Captive power plant (15 MW) of Meghalaya and Jaintia Cement Factory, respectively. The fly ash sample was sieved to particle size <75 μm and dried at 100 °C prior to the experiment. Quartz sands (<1 mm)

were collected from a river bed and were cleaned with 1 M HCl prior to the experiments in order to produce clean materials.

2.2 Material Characterization

Elemental analysis, mineralogical characterization, and surface morphology were carried out using an XRF spectrometer (Philips PW 2400), an X-ray diffractometer (Rigaku MiniFlex, Cu Kα radiation), a scanning electron microscope with an energy-dispersive spectroscopy (EDS) (JEOL SEM 5800), and an optical microscope. Acid-producing potential of sulfide residues was calculated by multiplying 31.25 with the weight percent of pyritic sulfur (Perry 1998).

Sulfide-rich waste contains high concentrations of S (50.33 % SO_3) and Fe (42.94 % Fe_2O_3) besides other elements in much lower quantities (Table 1). Pyrite is the major mineral phase in the sulfide waste and occurs as nodules, in the form of octahedral, framboidal, and porous (Fig. 1). The acid-producing capacity of this sulfide waste is 880 kg $CaCO_3$/t, which is classified as potentially acid generating based on the acid–base accounting criteria (Sobek et al. 1978).

The chemical compositions of fly ash (FA) and clinker dust (CD) are given in Table 1. The ash is silicoaluminous with 46.3 % SiO_2, 27.6 % Al_2O_3, 5.7 % Fe_2O_3, and 0.95 % CaO and trace amounts of Cu, Cd, Cr, Mn, Zn, and Pb. The mineralogy of ash includes quartz, anhydrite, and hematite as the dominant phases. CD is rich in CaO

Table 1 Chemical composition of sulfide waste, clinker dust, and fly ash

	SW	CD	FA
Major element (wt%)			
Al_2O_2	0.65	5.3	27.6
Fe_2O_2	42.9	2.0	5.70
SiO_2	3.74	21.9	46.3
MgO	0.07	2.97	0.30
CaO	0.09	62.5	0.95
Na_2O	0.21	0.4	0.67
K_2O	0.46	0.7	0.46
SO_3	50.3	0.9	–
Minor elements (mg/kg)			
Cu	43.4	1.8	106
Cd	5.5	0.3	87
Cr	44	10.2	61
Mn	180	16.7	80
Zn	103	1.4	220
Pb	45	0.7	119

SW sulfide waste, *CD* clinker dust, *FA* fly ash

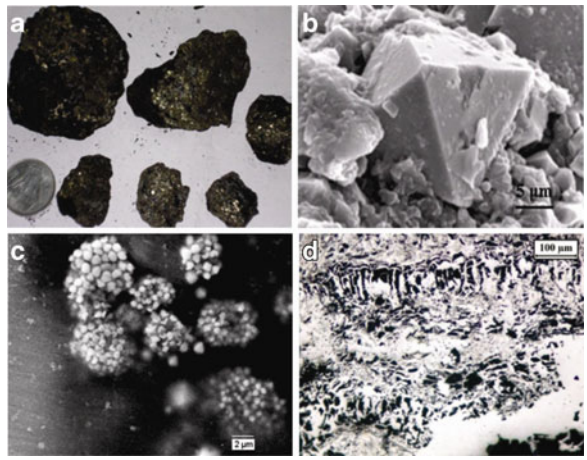

Fig. 1 Direct image of nodule pyrite (**a**), SEM image of octahedral (**b**) and framboidal pyrite (**c**), and petrographic image of porous pyrite

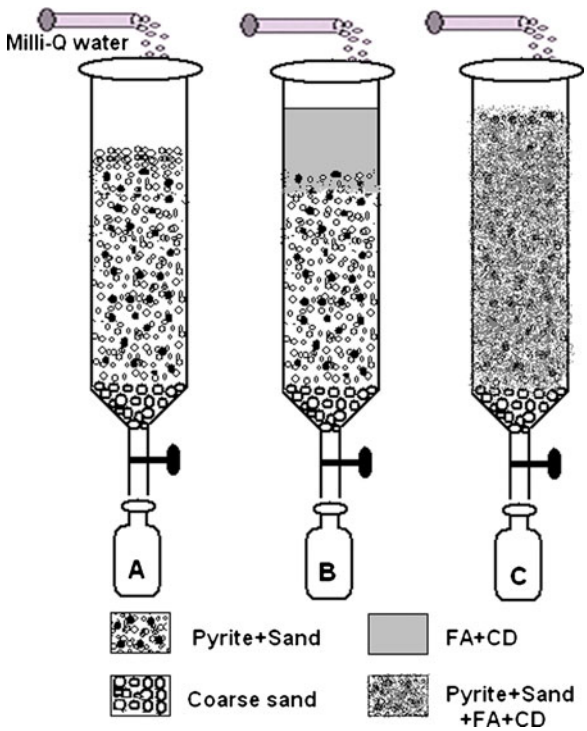

Fig. 2 Experimental design: non-saturated column filled with pyrite-quartz sand (**a**), pyrite-quartz sand with fly ash (*FA*)-clinker dust (*CD*) at the top (**b**), and pyrite-quartz sand homogenously mixed with FA–CD

(62.5 %) and SiO_2 (21.9 %) with minor amounts of Al_2O_3 (5.26 %), MgO (2.97 %), and Fe_2O_3 (2 %) along with trace amounts of Cu, Cd, Cr, Pb, and Mn (Table 1). Major mineral phases in CD are quartz and calcite. Although the toxic element concentrations can be high in fly ash, these elements are released in much lower concentrations than the concentration in AMD (Sahoo 2011). In addition, the alkaline pH generated from the fly ash mixture favors the depletion of these metals by precipitation or co-precipitation with Fe-oxyhydroxide minerals. Thus, utilization of this ash will not contribute to increase the contamination levels of the AMD.

3 Experimental Setup

Pyritic-bearing wastes in the Jaintia Hills are often highly permeable and non-saturated, where regular diffusion of atmospheric O_2 favors oxidation of large amounts of pyritic materials. In order to represent this condition in the laboratory, pyritic-bearing wastes were mixed with inert quartz sand, to simulate a porous mixture, and leached in non-saturated columns. The presence of quartz sand not only increases the permeability, but also stimulates the oxidation condition.

The experimental setup consists of three individual columns (A, B, and C), each 30 cm in length and 6 cm in diameter. Each column was filled with a mixture of 300 g of quartz sand and 30 g of pyrite. Column A was kept solely with pyrite-quartz sand (PS). In column B, a mixture of industrial residue (150 g of FA and 10 g CD) was loaded on top of the PS, whereas in column C, the same amount of industrial residue, as in the case of column B, was mixed homogeneously with PS. The proportion of above materials was fixed based on preliminary tests. The bottom of each column was loaded with sharp grains of quartz sand (1.4–4 mm) in order to facilitate the flow of the leachate. Each column had one inlet and one outlet. The schematic representation of the leaching columns is shown in Fig. 2. In order to simulate the precipitation, first 100 ml of Milli-Q water (pH 6.5) was manually poured at the beginning of the

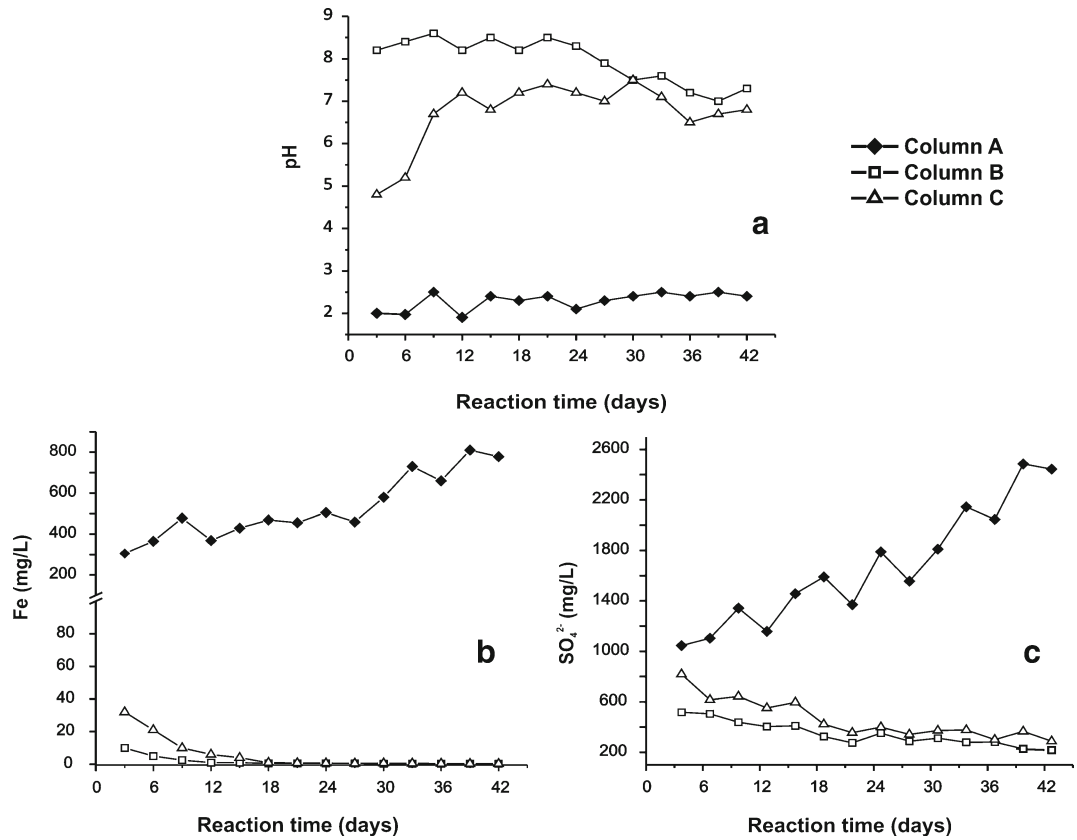

Fig. 3 Variation of pH (**a**), Fe (**b**), and SO_4^{2-} (**c**) vs time in the leachates of columns A, B, and C

experiment, and then, 25 ml of water was added in 3 days interval. The output leachates were collected at the end of every 3 days. The residence time of the first leachate is 3 days; thereafter, it might have changed. The water movement was manually observed in each column after pouring the input solution. All the experiments were carried out at 22 °C in an oxygen-saturated atmosphere and continued over a period of 42 days.

The pH was measured in the leachate immediately after collection using ion-selective electrodes (ORION model 1260). The leachate samples were subsequently filtered through 0.45-μm Whatman filter papers, acidified to pH <2 with suprapure HNO_3, and stored at 4 °C. Concentrations of metals such as Fe, Mn, Zn, Cr, and Pb in the leachates were measured by an atomic absorption spectrophotometer (PerkinElmer Analyst 300). The SO_4^{2-} concentration was measured by turbidimetric method (APHA 1995). The analytical errors were within ±10 % for all ions. After the experiments had terminated, the reacted pyrite and the neo-formed phases were collected from the columns and indentified by SEM-EDS.

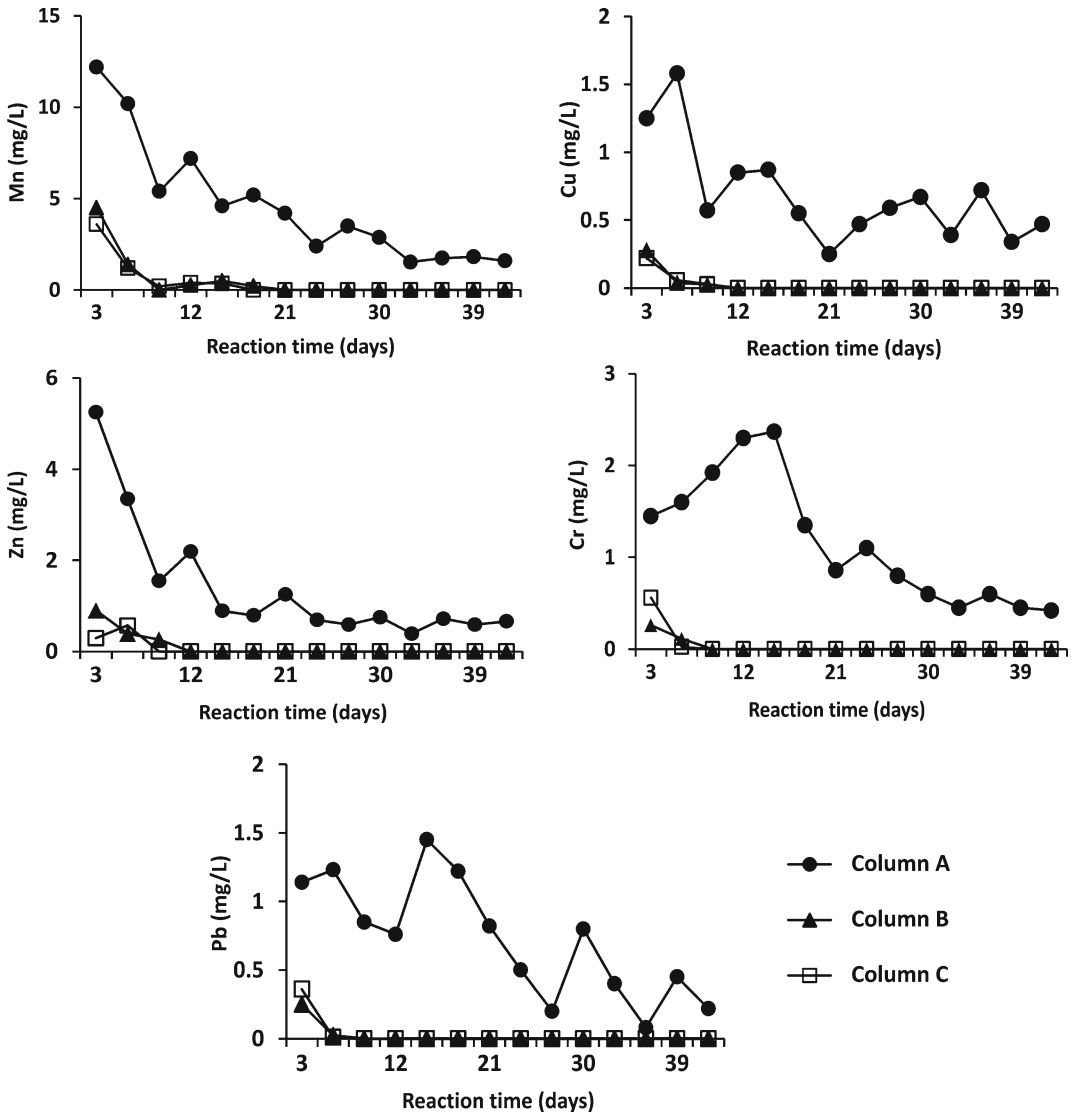

Fig. 4 Variation of Mn, Cu, Zn, Cr, and Pb in the leachates as a function of time

4 Geochemical Modeling (PHREEQC)

The saturation indices (SI) of various Fe-oxyhydroxides and calcium carbonate phases from the leachates were calculated using PHREEQC geochemical code (Parkhurst and Appelo 1999). The SI was calculated based on the following equation: SI=log (IAP/Ks), where IAP is the ion activity product of the dissolved components in the solution and Ks is the theoretical solubility product. H-jarosite data base was accessed from MINTEQ.dat file, while other Fe-oxyhydroxides and calcium carbonate phases were already in the PHREEQC.dat file (Parkhurst and Appelo 1999). An SI value of zero indicates that the mineral is in equilibrium in the solution and may either precipitate or dissolve. A positive SI value signifies that solution is supersaturated, while a negative SI indicates that the solution is undersaturated (Parkhurst and Appelo 1999).

5 Results

5.1 Leachate Chemistry

The pH of the leachates remained nearly constant during the entire time in column A (control) and column B, while in column C, there was initial decrease in pH followed by gradual increase till the 12th day and remained more or less constant thereafter (Fig. 3a). In the control column, the mean value of the leachate pH was 2.2, whereas in treated columns, this value increased to 8.2 and 7.8 in columns B and C, respectively.

The concentrations of SO_4^{2-} and Fe (Fig. 3b, c) increased more than double from 1,046 and 305 mg/L to 2,486 and 810 mg/L, respectively, with time in the leachate of column A. This is in contrast with those generated from columns B and C. Concentration of SO_4^{2-} gradually decreased in both columns B and C until steady state was attained after approximately 21 days. However, SO_4^{2-} concentration was higher in the leachate from column B than column C up to 15 days and remained unchanged thereafter. This indicates oxidation of pyrite being rapid within these 15 days in column B as compared to column C. The concentration of Fe in columns B and C is totally depleted after about 15 days than in column A, though the initial concentration was higher in column C than column B.

Further, concentrations of Mn, Zn, Pb, Cu, and Cr in the leachates (Fig. 4) of column A ranged from 12.2 to 1.6, 5.2 to 0.6, 1.14 to 0.2, 1.25 to 0.47, and 1.45 to 0.56 mg/L, respectively. Similar to Fe, these metal concentrations are much lower in the leachates of columns B and C compared to column A. Despite all three columns having similar amount of sulfide waste, the addition of FA and CD produced an improvement in the quality of the leachates in columns B and C.

6 Discussion

6.1 Column A

The leachates generated from this column yielded a highly acidic pH along with higher concentrations of Fe and SO_4^{2-}. This indicates continuous oxidation of pyrite from sulfide wastes in non-saturated porous media with continuous diffusion of atmospheric oxygen. The leachates are chemically similar to the typical acid mine discharge, and the oxidation process in this column can be related with the natural oxidation of sulfide residue of the Jaintia Hills. A very high proportion of metals (Ni, Cu, Pb, Mn, and Zn) in the leachates is due to the oxidation of pyrite from sulfide wastes. The

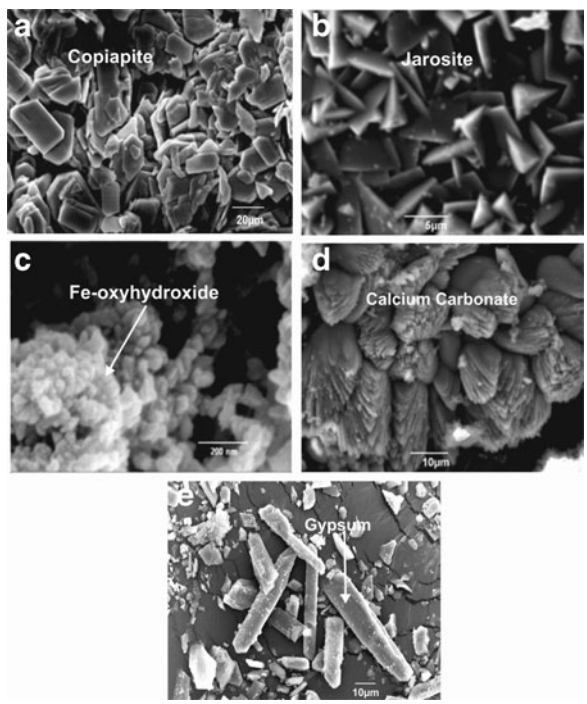

Fig. 5 Scanning electron micrographs of ferricopiapite (**a**), jarosite (**b**), other Fe-oxyhydroxides (**c**), calcium carbonate (**d**), and gypsum (**e**)

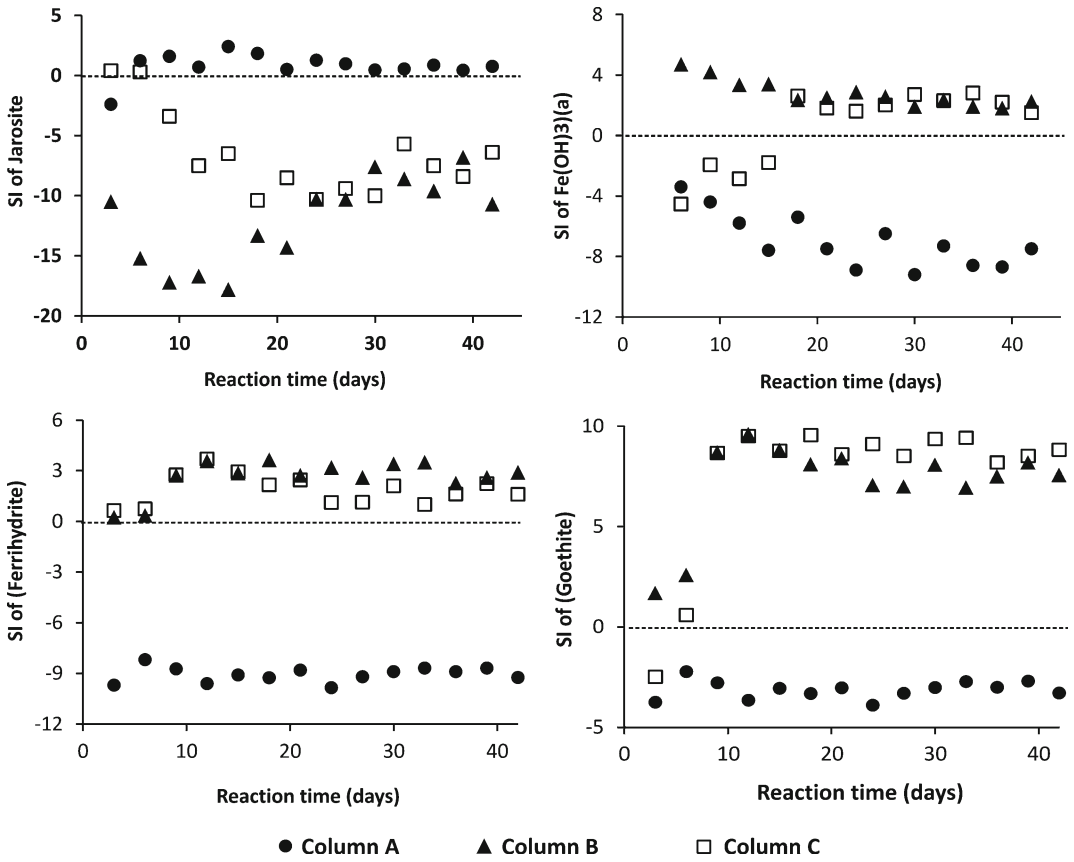

Fig. 6 Saturation index (*SI*) of jarosite, $Fe(OH)_{3(a)}$, ferrihydrite, and goethite calculated using the PHREEQC code (Parkhurst and Appelo 1999)

concentrations being highest at the beginning may be due to fast dissolution of Fe-sulfate salts (Hammarstroma et al. 2005). These salts are easily formed as sulfide oxidation products in a dry environment and can immediately return to solution in contact with water because of their high solubility (Hammarstroma et al. 2005). Thus, they can temporarily control the leachate chemistry. Precipitation of secondary sulfate minerals such as ferricopiapite ($Fe^{2+}Fe_4^{3+}(SO_4)_6(OH)_2$) was also observed in this column by SEM (Fig. 5a). Further, PHREEQC saturation index calculations show the solutions were saturated with respect to jarosite (Fig. 6), which was also identified by SEM (Fig. 5b). However, the precipitation of this phase only retains a very low proportion of metals. This may be due to a highly acidic pH which favors high mobility of metals in solution (Onundi et al. 2010).

6.2 Column B

The leachates from column B remained alkaline throughout in contrast to that of column A (Fig. 3a). This is due to the effect of calcium carbonate and calcium hydroxide

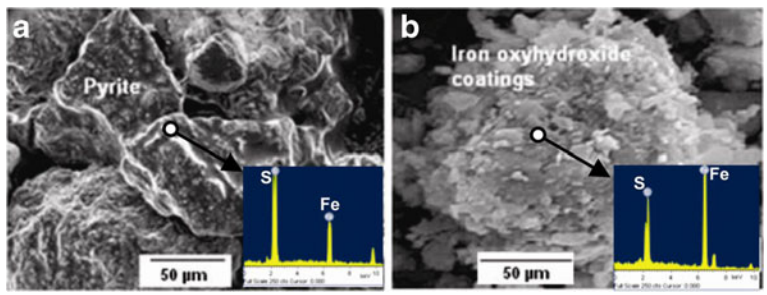

Fig. 7 Scanning electron microscope images of pyrite grain before (**a**) and after the experiment (**b**)

(Canty and Everett 2006), which are caused by the interaction of CaO in clinker dust and water in the environment (reactions 1 and 2). Dissociation of these two compounds increases the pH. However, with time, the pH slightly decreased (Fig. 3a), which may be due to the dissolution of carbonic acid along with depletion of lime. As the experiment is conducted in the atmospheric condition, it is expected that CO_2 dissolves in the alkaline water and forms carbonic acid (reaction 3) which further dissociates into bicarbonate and carbonate ions (reaction 4) until the equilibrium exists between the dissolved CO_2 and H_2CO_3.

$$CaO(\mathrm{s}) + CO_2 \rightarrow CaCO_3(\mathrm{s}) \quad (1)$$

$$CaO(\mathrm{s}) + \mathrm{H_2O} \rightarrow Ca(OH)_2(\mathrm{s}) \quad (2)$$

$$CO_2(\mathrm{g}) + \mathrm{H_2O} \leftrightarrow CO_2(aq) \leftrightarrow \mathrm{H_2}CO_3 \quad (3)$$

$$\mathrm{H_2}CO_3 \leftrightarrow \mathrm{H^+} + HCO_3 \leftrightarrow \mathrm{H^+} + {CO_3}^{2-} \quad (4)$$

The calcium carbonate and calcium hydroxide compounds not only increase pH, but also neutralize the resultant acidity (reactions 5 and 6) produced due to pyrite oxidation (Bulusu et al. 2007):

$$Ca(OH)_2(aq) + \mathrm{H_2}SO_4 \rightarrow Ca^{2+} + {SO_4}^{2-} + 2\mathrm{H_2O} \quad (5)$$

$$CaCO_3(aq) + \mathrm{H_2}SO_4 \rightarrow Ca^{2+} + {SO_4}^{2-} + CO_2(\mathrm{g}) + \mathrm{H_2O} \quad (6)$$

Under alkaline pH conditions when pyrite oxidizes, the released Fe rapidly precipitates as poor Fe-oxyhydroxide phases such as ferrihydrite and goethite (Yee et al. 2006). Since the point of zero charge of the Fe-oxyhydroxide colloid (Schick 2001) and pyrite (Bebie et al. 1998) is near about 9 and 1.4, respectively, it is expected that the Fe-oxyhydroxide colloid, which has a positive surface charge, is attracted to the negatively charged pyrite surface forming a thin layer on pyrite surface. In addition, these Fe-oxide phases are not soluble at alkaline pH. So, they encapsulate the pyrite grain completely with time and forbid any contact between the oxidant and pyrite surface and subsequently inhibit the oxidation process. This mechanism is termed as microencapsulation/passivation (Evangelou 1995). This causes a decrease in the pyrite oxidation with time as shown by the decrease of Fe and ${SO_4}^{2-}$ concentration with time (Fig. 3b, c). The Fe-oxyhydroxide coating on pyrite grain is observed by SEM-EDS analysis (Fig. 7). The EDS pattern of the pyrite grain after the experiment shows a progressive enrichment of Fe compared to the pattern before the experiment. An increase in Fe with respect to S indicates that an excitation zone is much more superficial and it does not penetrate into the pyrite

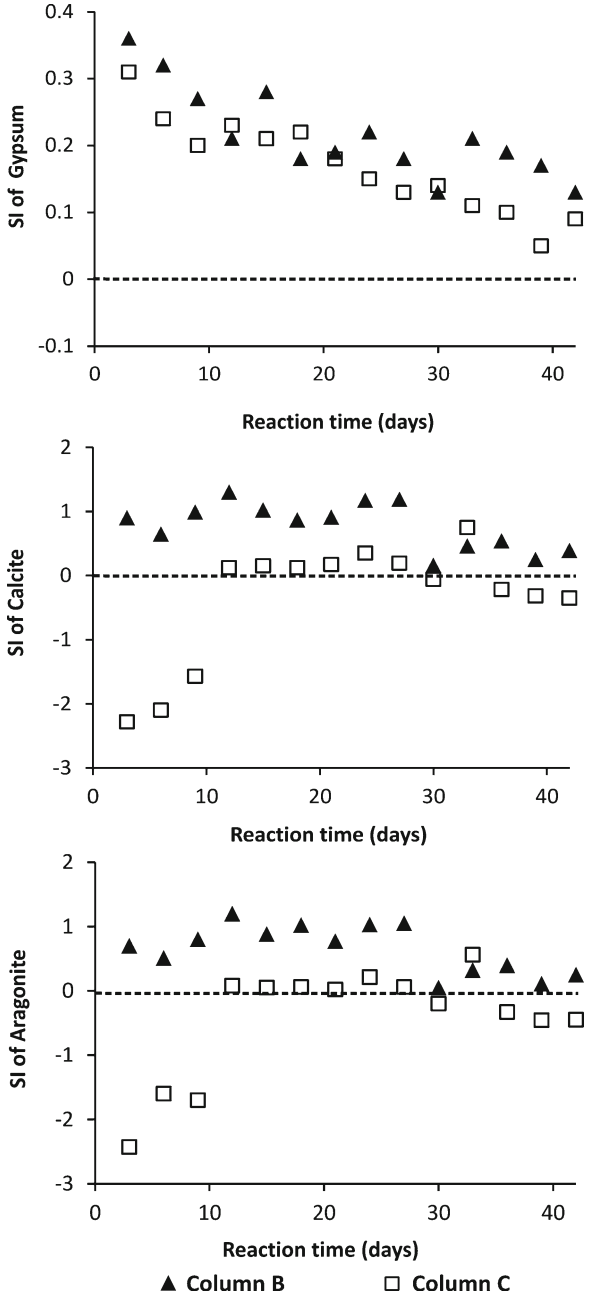

Fig. 8 Saturation index (*SI*) of gypsum, calcite, and agaronite in columns B and C using the PHREEQC equation (Parkhurst and Appelo 1999)

grain (Pérez-López et al. 2007b). Thus, the phases covering the pyrite grains are Fe bearing. Calculation with PHREEQC also shows the leachates are supersaturated with respect to Fe-oxyhydroxide phases such as $Fe(OH)_{3(a)}$, ferrihydrite, and goethite (Fig. 6). Very low concentrations of the metals (Mn, Zn, Pb, Cr, and Cu) were observed in the leachates of this column, which comply with the WHO drinking water quality stipulation (WHO 1993). This low concentration may be due to the alkaline pH and precipitation of various Fe-oxyhydroxide phases, which scavenge the metals because of their high sorption capacity (Sahoo et al. 2012b; McGregor et al. 1998). Perez-Lopez et al. (2007a) also demonstrated that the addition of fly ash on pyrite-rich residues increased leachate pH that leads to precipitation of secondary Fe phases and significantly decreases concentrations of metals from the leachates.

Furthermore, during the experiment, amorphous calcium carbonate (ACC) and gypsum also precipitated as other neo-formed minerals that were indentified (Fig. 5d, e). ACC is a poorly ordered phase which immediately precipitates due to continuous diffusion of atmospheric CO_2 and the high concentrations of Ca and then transforms to crystalline polymorphs, such as calcite, aragonite, and vaterite (Rodriguez-Blanco et al. 2012). The PHREEQC calculation shows the leachates are saturated with respect to carbonate phases, such as aragonite and calcite, and gypsum (Fig. 8). The intense precipitation of ACC at the top layer of fly ash occurred as massive cement with ash particles leading to the formation of a hard crust or hardpan. This resulted in a decrease (qualitative) in the movement of water in the column and an increase in time of contact of water with the mineral grains. Further, gypsum is developed at the interface between the fly ash and pyrite sand zone. The detailed role of neo-formed phases is shown in a schematic drawing (Fig. 9a).

Additionally, the presence of clinker dust may also activate the pozzolanic reactions, where CaO is converted to $Ca(OH)_2$ in the presence of water and then react with silica and aluminum oxide to produce cementitious materials such as calcium silicate gel (reaction 7) and calcium aluminate gel, which is capable of binding inert solid particles and leads to form a hardened material (Palamo et al. 2007).

$$2SiO_2 + 3Ca(OH)_2 \rightarrow 3CaO\cdot 2SiO_2 3H_2O \quad (7)$$

Precipitation of neo-formed phases and the calcium silicate hydrate at the interface can develop a hardpan, which over time becomes harder like cement and forms a physical barrier to water flow. This is observed with an increase in time for the input solutions to flow inside the column. Many authors previously reported the formation of hardpan in the contact zone of alkaline substance and acid-producing waste (Chermak and Runnells 1997; Ding et al. 2002; Pérez-López 2007b, c). This hardpan can favor isolation of mine waste from weathering, create a physical barrier to ingress of water and atmospheric oxygen into the pyrite waste, and hinder further pyrite oxidation.

6.3 Column C

Like column B, the leachates of column C are of near neutral to alkaline pH except the first three samples and low Fe and SO_4^{2-} concentrations. Leachates are supersaturated with respect to Fe-oxyhydroxide phases ($Fe(OH)_{3(a)}$, goethite, and ferrihydrite in this column (Fig. 6), which leads to the removal of Fe, SO_4^{2-}, and other metals. Moreover, these phases inhibit the oxidation processes by forming a coating on the pyrite grain

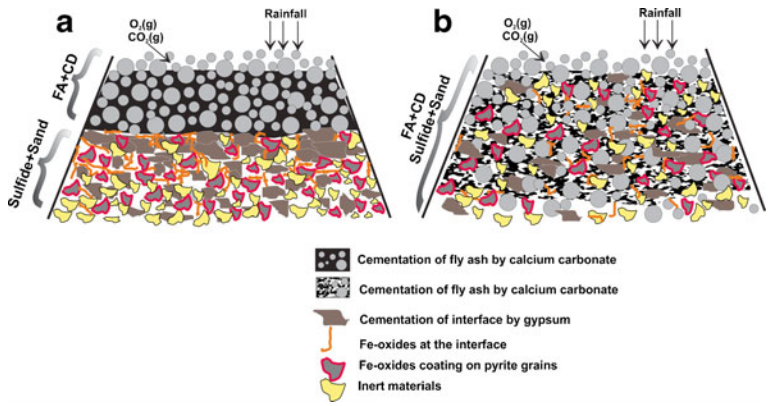

Fig. 9 Scheme showing the Fe-oxide coating on pyrite grains and precipitation of neo-formed phases at the interface in columns B (**a**) and C (**b**)

(microencapsulation). In addition, other neo-formed secondary minerals (e.g., calcium carbonate and gypsum) were also formed in the void zones. However, the precipitation of calcium carbonate was of less extent compared to column B. It is also observed from the SI index values (Fig. 8), as the alkaline material is mixed homogenously with the pyrite mixture. As such, no hardpan was formed in this column (Fig. 9b); thus, easy water movement occurred in this column, which further oxidized pyrite. This may be the cause for higher concentrations Fe and SO_4^{2-} in the leachates of this column compared to column B. Although the leachate quality improved with time and complied with WHO drinking water quality stipulation (WHO 1993), the absence of hardpan in this column can allow further oxidation; thus, the process used in this column is comparatively less effective in mitigating AMD than column B.

7 Conclusions

In this study, the effectiveness of the mixture of industrial wastes (fly ash and clinker dust) in inhibiting pyrite oxidation and resultant AMD generation from a pyrite-rich mine residue has been demonstrated by column leaching experiments. The application of industrial wastes to the pyrite-rich residues in columns B and C decreased the pyrite oxidation by releasing alkaline solution and removing SO_4^{2-}, Fe, and other metals, viz. Mn, Zn, Pb, Cu, and Cr, from the solution which resulted from the pyrite oxidation. Inhibition of pyrite oxidation is a consequence of Fe-oxyhydroxide coating on pyrite surface and precipitation of neo-formed phases at the interface and surfaces leading to hardpan formation, which act as a physical barrier to water flow and diminish the oxygen diffusion to the entire column, thereby resulting in an improvement in the quality of the leachate. Although by the end of the experiment the leachate quality was almost alike in both columns, hardpan formation only occurred in column B; therefore, the technique used in column B would be more effective to mitigate the AMD generation than column C.

Acknowledgments The authors sincerely thank the two anonymous reviewers for their thorough reviews and constructive comments, which significantly improved the quality of this manuscript. PKS is thankful to Dr. S. Dutta, State Pollution Control Board, Meghalaya for arranging the fly ash sample. Instrumental support for SEM analysis was availed from the Central Research Facility of IIT Kharagpur.

References

Ačai, P., Sorrenti, E., Polakovič, M., Kongolo, M., & Donato, P. D. (2009). Pyrite passivation by humic acid investigated by inverse liquid chromatography. *Colloids and Surfaces A: Physicochemical and Engineering Aspects, 337*, 39–46.

Akabzaa, T. M., Armah, T. E. K., & Baneong-Yakubo, B. K. (2007). Prediction of acid mine drainage generation potential in selected mines in the Ashanti Metallogenic Belt using static geochemical methods. *Environmental Geology, 52*, 957–964.

APHA. (1995). *Standard methods for the examination of water and waste water* (19th ed.). Washington, DC: American Public Health Association.

Bebie, J., Schoonen, M. A. A., Fuhrmann, M., & Strongin, D. R. (1998). Surface charge development on transition metal sulfides: an electrokinetic study. *Geochimica et Cosmochimica Acta, 62*, 633–642.

Belzile, N., Maki, S., Chen, Y. W., & Goldsack, D. (1997). Inhibition of pyrite oxidation by surface treatment. *The Science of the Total Environment, 196*, 177–186.

Bulusu, S., Aydilek, H. A., & Rustagi, N. (2007). CCB-based encapsulation of pyrite for remediation of acid mine drainage. *Journal of Hazardous Materials, 143*, 609–619.

Cai, M. F., Dang, Z., Chen, Y. W., & Belzile, N. (2005). The passivation of pyrrhotite by surface coating. *Chemosphere, 61*, 659–667.

Campbell, R. N., Lindsay, P., & Clemens, A. H. (2001). Acid generating potential of waste rock and coal ash in New Zealand coal mines. *International Journal of Coal Geology, 45*, 163–179.

Canty, G. A., & Everett, J. W. (2006). Injection of fluidized bed combustion ash into mine working for treatment of acid mine drainage. *Mine Water and the Environment, 25*, 45–55.

Chermak, J. A., & Runnells, D. D. (1997). Development of chemical caps in acid rock drainage environments. *Mining Engineering, 49*, 93–97.

Ding, M., Schuiling, R. D., & van der Sloot, H. A. (2002). Self-sealing isolation and immobilization: a geochemical approach to solve the environmental problem of waste acidic jarosite. *Applied Geochemistry, 17*, 93–103.

Equeenuddin, S. M., Tripathy, S., Sahoo, P. K., & Panigrahi, M. K. (2010). Hydrogeochemical characteristics of acid mine drainage and water pollution at Makum Coalfield, India. *Journal of Geochemical Exploration, 105*, 75–82.

Evangelou, V. P. (1995). *Pyrite oxidation and its control*. New York: CRC.

Evangelou, V. P. (2001). Pyrite microencapsulation technologies: principles and potential field application. *Ecological Engineering, 17*, 165–178.

Hammarstroma, J. M., Seal, R. R., Meier, A. L., & Kornfeldc, J. M. (2005). Secondary sulfate minerals associated with acid drainage in the eastern US: recycling of metals and acidity in surficial environments. *Chemical Geology, 215*, 407–431.

Ji, S. W., Cheong, Y. W., Yim, G. J., & Bhattacharya, J. (2007). ARD generation and corrosion potential of exposed roadside rockmass at Boeun and Mujoo, South Korea. *Environmental Geology, 52*, 1033–1043.

Johnson, D. B., & Hallberg, K. B. (2005). Acid mine drainage remediation options: a review. *Science of the Total Environment, 338*, 3–14.

Kargbo, D. M., Atallah, G., & Chatterjee, S. (2004). Inhibition of pyrite oxidation by a phospholipid in the presence of silicate. *Environmental Science and Technology, 38*, 3432–3441.

Kleinmann, R. L. P. (1990). At-source of acid mine drainage. *Mine Water and the Environment, 9*, 85–96.

Kleinmann, R. L. P. (1998). Bactericidal control of acidic drainage. In K. C. Brady, M. W. Smith, & J. Schueck (Eds.), *Coal mine drainage prediction and pollution prevention in Pennsylvania* (Vol. 15, pp. 1–6). Harrisburg: PA DEP.

Lottermoser, B. (2007). Mine wastes characterization, treatment and environmental impacts, 2nd edition. Springer, Heidelberg.

McGregor, R. G., Blowes, D. W., Jambor, J. L., & Robertson, W. D. (1998). The solid-phase controls on the mobility of heavy metals at the Copper Cliff tailing area, Sudbury, Ontario. *Journal of Contaminant Hydrology, 33*, 247–271.

Nordstrom, D. K., & Alpers, C. N. (1999). Negative pH, efflorescent mineralogy, and consequences for environmental restoration at the Iron Mountain Superfund site, California. *Proceedings of the National Academy of Sciences USA, 96*, 3455–3462.

Nyavor, K., & Egiebor, N. O. (1995). Control of pyrite oxidation by phosphate coating. *The Science of the Total Environment, 162*, 225–237.

Onundi, Y. B., Mamun, A. A., Khatib, M. F. A., & Ahmed, Y. M. (2010). Adsorption of copper, nickel and lead from synthetic semiconductor industrial wastewater by palm shell activated carbon. *International Journal of Environmental Science and Technology, 7*, 751–758.

Palamo, A., Fernaddez-Jimenez, A., Kovalchuk, G., Ordonez, L. M., & Naranjo, M. C. (2007). Opc-fly ash cementitious systems: study of gel binder produced during alkaline hydration. *Journal of Materials Science, 42*, 2958–2966.

Parkhurst, D. L., & Appelo, C. A. J. (1999) User's guide to PHREEQC (version 2)—a computer program for speciation, batch-reaction, one-dimensional transport, and inverse geochemical calculations. USGS Water-Resources Investigations Report 99–4259.

Pelo, D. S., Musu, E., Cidu, R., Frau, F., & Lattanzi, P. (2009). Release of toxic elements from rocks and mine wastes at the Furtei gold mine (Sardinia, Italy). *Journal of Geochemical Exploration, 100*, 142–152.

Pérez-López, R., Nieto, J. M., & Almodovar, G. R. (2007a). Utilization of fly ash to improve the quality of the acid mine drainage generated by oxidation of a sulfide-rich mining waste: column experiments. *Chemosphere, 67*, 1637–1646.

Pérez-López, R., Cama, J., Nieto, J. M., & Ayora, C. (2007b). The iron-coating role on the oxidation kinetics of a pyritic sludge doped with fly ash. *Geochimica et Cosmochimica Acta, 71*, 1921–1934.

Pérez-López, R., Nieto, J. M., Alvared-valero, A. M., & Almodovar, G. R. (2007c). Mineralogy of the hardpan formation processes in the interface between sulfide-rich sludge and fly ash: applications for acid mine drainage mitigation. *American Mineralogist, 92*, 1966–1977.

Perry, E. (1998). Interpretation of acid-base accounting. Chapter 11. In *Coal mine drainage prediction and pollution prevention in Pennsylvania*. Pennsylvania Dept of Environ Protection, Harrisburg.

Perry, E. F., & Brady, K. B. C. (1995). Influence of neutralization potential on surface mine drainage in Pennsylvania. In: Proceedings Sixteenth Annual West Virginia Surface Mine Drainage Task Force Symposium, Morgantown, West Virginia.

Rodriguez-Blanco, J. D., Shaw, S., Bots, P., Roncal-Herrero, T., & Benning, L. G. (2012). The role of pH and Mg on the stability and crystallization of amorphous calcium carbonate. *Journal of Alloys and Compounds, 536*, S477–S479.

Sahoo P. K. (2011). Geochemical appraisal of acid mine drainage around Jaintia Hills coalfield, Meghalaya, India, Unpublished PhD Thesis, Indian Institute of Technology, Kharagpur.

Sahoo, P. K., Tripathy, S., Equeendduin, S. M., & Panigrahi, M. K. (2012a). Geochemical characteristics of coal mine discharge vis-à-vis behavior of rare earth elements at Jaintia Hills Coalfield, Northeastern India. *Journal of Gechemical Exploration, 112*, 235–243.

Sahoo, P. K., Tripathy, S., Panigrahi, M. K., & Equeenuddin, S. M. (2012b). Mineralogy of Fe-precipitates and their role in metal retention from an acid mine drainage site in India. *Journal of Mine Water and Environment, 31*, 344–352.

Sahoo, P. K., Tripathy, S., Panigrahi, M. K., & Equeenuddin, S. M. (2013). Evaluation of the use of an alkali modified fly ash as a potential adsorbent for the removal of metals from acid mine drainage. *Applied Water Science, 3*, 567–576.

Schick, M. J. (2001). Chemical properties of material surfaces. In A. T. Hubbard (Ed.), *Surfactant science series*. New York: Marcel Dekker.

Singer, P. C., & Stumm, W. (1970). Acidic mine drainage—the rate-determining step. *Science, 167*, 1121–1123.

Sobek, A. A., Schuller, W.A., Freeman, J.R., & Smith, R. M. (1978). Field and laboratory methods applicable to overburden and minesoils, EPA 600/2-78-054, 203 p.

Tasse, N., Germain, D., Dufour, C., & Tremblay, R. (1997). Hard-pan formation in the Canadian Malartic mine tailings: implication for the reclamation of the abandoned impoundment. In: Proceeding of Fourth International Conference on Acid Rock Drainage. Vancouver, B.C, Canada, Vol. III, pp 1797−1812.

Vandiviere, M. M., & Evangelou, V. P. (1998). Comparative testing between conventional and microencapsulation approaches in controlling pyrite oxidation. *Journal of Geochemical Exploration, 64*, 161–176.

Vigneault, B., Campbell, P. G. C., Tessier, A., & Vitre, R. D. (2001). Geochemical changes in sulfide mine tailings stored under a shallow water cover. *Water Research, 35*, 1066–1076.

WHO (1993). *Guidelines for drinking water quality: recommendations*, vol. 1. World Health Organization, Geneva.

Yanful, E. K., Orlandea, M. P., & Eliasziw, M. (2000). Controlling acid drainage in a pyrite mine waste rock. Part I: statistical analysis of drainage data. *Water, Air, and Soil Pollution, 122*, 369–388.

Yee, N., Shaw, S., Benning, L. G., & Hien Nguyen, T. (2006). The rate of ferrihydrite transition to goethite via the Fe(II) pathway. *American Mineralogist, 91*, 92–96.

Zhang, Y. L., & Evangelou, V. P. (1998). Formation of ferric hydroxide–silica coatings on pyrite and its oxidation behavior. *Soil Science, 163*, 53–62.